ARTICLES
https://doi.org/10.1038/s41563-021-01111-2

nature materials

Check for updates

3D-printed silica with nanoscale resolution

Xiewen Wen[1,5], Boyu Zhang[1,5], Weipeng Wang[1,2]✉, Fan Ye[3], Shuai Yue[4], Hua Guo[1], Guanhui Gao[1], Yushun Zhao[1], Qiyi Fang[1], Christine Nguyen[1], Xiang Zhang[1], Jiming Bao[4], Jacob T. Robinson[3]✉, Pulickel M. Ajayan[1]✉ and Jun Lou[1]✉

Fabricating inorganic materials with designed three-dimensional nanostructures is an exciting yet challenging area of research and industrial application. Here, we develop an approach to 3D print high-quality nanostructures of silica with sub-200 nm resolution and with the flexible capability of rare-earth element doping. The printed SiO_2 can be either amorphous glass or polycrystalline cristobalite controlled by the sintering process. The 3D-printed nanostructures demonstrate attractive optical properties. For instance, the fabricated micro-toroid optical resonators can reach quality factors (*Q*) of over 10^4. Moreover, and importantly for optical applications, doping and codoping of rare-earth salts such as Er^{3+}, Tm^{3+}, Yb^{3+}, Eu^{3+} and Nd^{3+} can be directly implemented in the printed SiO_2 structures, showing strong photoluminescence at the desired wavelengths. This technique shows the potential for building integrated microphotonics with silica via 3D printing.

Nanostructured inorganic materials with promising potential applications have drawn tremendous research attention from both fundamental and practical aspects. SiO_2 (silica) is one of the most widely used inorganic materials and demands fabrication methods with nanoscale resolution in fields such as microelectronics[1,2], microelectromechanical systems[3,4] and microphotonics[5,6]. To fabricate silica with desired nanostructures, complicated top-down patterning processes including thermal oxidation[7] and chemical vapour deposition[8], followed by either dry[9,10] or wet[11,12] etching steps, are normally required. Although mature processing techniques with high yield have been developed, these techniques involve the use of hazardous chemicals (for example, resists, developers and etchants) and require complex facilities for fabrication. Moreover, achieving intricate and/or asymmetric three-dimensional (3D) architectures at nanometre resolution is very challenging using top-down fabrication methods. Therefore, large demand exists for direct nano-manufacturing techniques that can produce 3D silica structures with complex geometries and chemical variabilities.

The emerging technology of additive manufacturing (AM), or 3D printing using digital designs, can create fine structures through layer-by-layer deposition[13–16] to generate complex architectures and simplify fabrication processes. More importantly, as a well-demonstrated bottom-up technique, 3D printing has been reported to construct curvilinear substrates[17], nonplanar surfaces[18] and tortuous 3D patterns[19] that are beyond the capability of traditional top-down patterning methods. AM of fused silica glass was realized via stereolithography of an amorphous silica-rich slurry[20] with a resolution of tens of micrometres. Although well-defined structures with outstanding optical and mechanical properties were manufactured, the relatively low spatial resolution offered by commercial 3D-printing techniques limits their application in microelectronics, microelectromechanical systems and microphotonics. The emerging techniques of micro-digital-light-processing[21,22] have been implemented to improve the spatial resolution below 10 micrometres. However, this is still not adequate for microphotonic device applications that require a spatial resolution smaller than the wavelength of light.

Subwavelength spatial resolution can be attained via two-photon polymerization (2PP)[23], a laser-based direct writing technology in which the resin initiates free radical polymerization by simultaneously absorbing two photons. Since the two-photon absorption process is able to overcome the optical limit of illumination, subwavelength spatial resolution can be readily achieved. The 2PP-enabled AM techniques using photopolymers[24,25] have been widely used to fabricate nanostructures with intricate architectures. Very few AM techniques utilizing hybrid organic–inorganic materials[26] and polymer-derived ceramics[27,28] have been reported. Such inorganic nanostructures greatly broaden the application range of 2PP AM. However, they often contain mixtures of carbon or nitrogen elements with complex molecular compositions that present less-controllable electrical properties and lack optical transparency. This hinders their application in microelectronics and micro-/nanophotonics. To address these limitations, we propose an approach to 3D print silica nanostructures with sub-200 nm resolution. Additionally, the 3D-printed inorganic nanostructures were doped with desired rare-earth elements, which expand the applications to active photonics[29], non-Hermitian photonics[30] and quantum devices[31]. The technique involves 2PP-enabled AM of well-dispersed poly (ethylene glycol) (PEG)-functionalized colloidal silica nanocomposite ink, followed by pyrolysis and sintering, where the postprocessing procedure determines the crystallinity of the structures produced.

In our proposed technique, making a suitable 'ink' containing silica nanoparticles (NPs) and a two-photon polymerizable precursor is the dominating factor. Such ink must meet several conditions: first, the size of silica NPs has to be small (about 10 nm) to achieve nanoscale resolution; second, the refractive index of the photopolymer precursor must match that of silica to obtain transparent ink to eliminate photo extinction and scattering; third, the heat conductivity of the ink must be high to avoid instant vaporization by the femtosecond laser with megawatts of peak power; fourth, the

[1]Department of Materials Science and NanoEngineering, Rice University, Houston, TX, USA. [2]Key Laboratory of Advanced Materials (MOE), School of Materials Science and Engineering, Tsinghua University, Beijing, P. R. China. [3]Department of Electrical and Computer Engineering, Rice University, Houston, TX, USA. [4]Department of Electrical and Computer Engineering, University of Houston, Houston, TX, USA. [5]These authors contributed equally: Xiewen Wen, Boyu Zhang. ✉e-mail: wpwang@tsinghua.edu.cn; jacob.t.robinson@rice.edu; ajayan@rice.edu; jlou@rice.edu

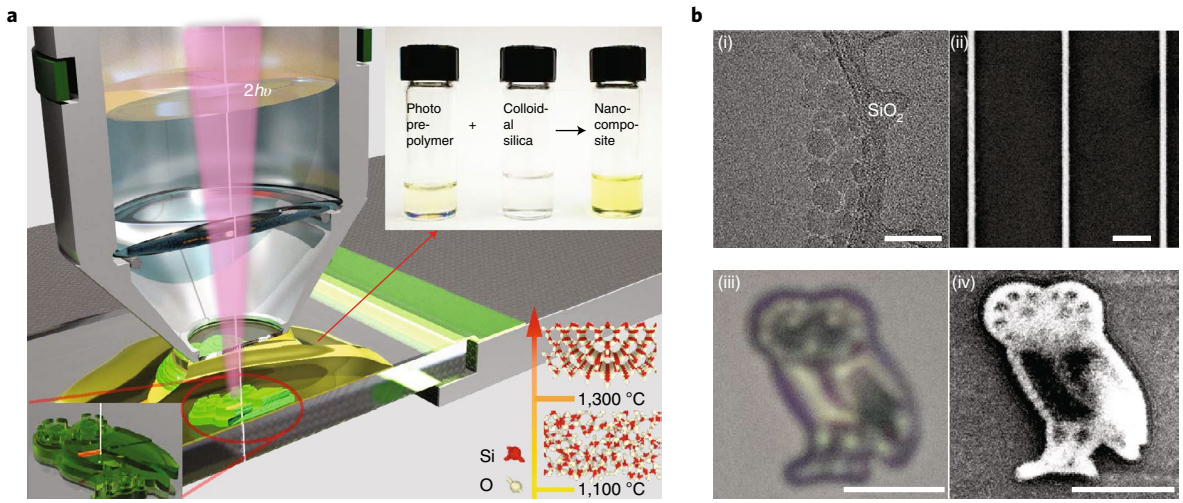

Fig. 1 | Process of 2PP-enabled 3D printing of silica. a, Schematic of 2PP-enabled 3D-printing set-up and printing process. *h* and ν are Planck's constant and the frequency of the laser, respectively. $2h\nu$ represents two photons absorbed by the nanocomposite. Upper right inset: photo of the as-synthesized polymer precursors, the colloidal silica NPs and the as-synthesized nanocomposite ink. Bottom left inset: cartoon of the printed Rice Owls structure. Bottom right inset: atomic structures of silica under different sintering temperatures. **b**, Microscopic images. TEM image of typical morphology of the silica NPs showing average diameter of 11.5 nm ((i); scale bar, 40 nm); the SEM image of the printed lines after sintering ((ii); scale bar, 1 μm); optical microscope image of the printed Rice Owls figure after sintering ((iii); scale bar, 5 μm); and SEM image of the printed Rice Owls figure after sintering ((iv); scale bar, 5 μm).

ink must be very homogeneous and well dispersed to maintain nanoscale resolution as well as to avoid localized vaporization; and fifth, the mass loading of the silica NPs should be high to maintain the printed geometry and minimize deformation. Simultaneously meeting all of the above conditions is challenging. For example, though using smaller NPs is necessary to achieve high-resolution, submicrometre-size particles can result in an undesirable mixture with high viscosity, which in turn makes mechanical mixing difficult. Additionally, high viscosity also leads to low heat conductivity because viscosity is normally inversely proportional to heat conductivity[32]. To resolve these conflicts, our strategy is to use PEG-functionalized well-dispersed colloidal silica NPs and a mixture of two small-molecule acrylate precursors. To maintain the consistency across multiple experiments and minimize the influence of NP quality on the results, we chose to use commercially available PEG-functionalized silica NPs. PEG functional groups are chemically attached to the colloidal silica NPs, which is confirmed by the Fourier transform infrared spectrum of dried functionalized NPs. As shown in Supplementary Fig. 1e, a new peak emerges at 1,703 cm^{-1}, corresponding to the stretching vibration of carbonyl groups from PEG, which agrees well with the literature[33]. The polymer precursors contain the same PEG functional group as colloidal silica NPs, which makes the silica NPs have excellent miscibility and dispersity in the polymer precursors. Moreover, the mixture of polymer precursors has the same refractive index as silica and can be fully removed during the subsequent annealing processes. Therefore, mixing colloidal silica NPs, polymer precursors and photo-initiator can produce well-dispersed nanocomposite ink with the silica NP size down to 10 nm with high loading (40 wt%), low viscosity, high transparency and high heat conductivity.

With the successful preparation of the nanocomposite ink and by employing the 2PP printing technique, we demonstrate that the final 3D-printed product is of pure silica with sub-200 nm resolution. Such fine spatial resolution is two orders of magnitude higher than the reported resolution that was recently achieved using a similar 2PP technique[34], and the use of PEG-functionalized colloidal silica NPs is considered to be crucial for achieving the nanoscale printing resolution. Depending on the sintering temperature, the final silica structures can be either amorphous glass or polycrystalline cristobalite, suggesting tunability of the optical properties of the printed structures. Using nanoscale silica glass, we demonstrated that micro-toroid optical resonators fabricated using the proposed technology have quality factors (Q) over 10^4. Furthermore, we showed that doping and codoping of rare-earth salts such as Er^{3+}, Tm^{3+}, Yb^{3+}, Eu^{3+} and Nd^{3+} can be directly implemented in the printed silica structures. The final doped silica glass nanostructure demonstrated strong photoluminescence at the desired wavelengths. Especially for Er^{3+}, the final printed structures exhibit photoluminescence around 1.55 μm, making the proposed technology a powerful tool for optical telecommunication applications.

The solution of PEG-functionalized well-dispersed colloidal silica NPs with an average diameter of 11.5 nm (Fig. 1b(i) and Supplementary Fig. 1) is mixed with two carefully selected small-molecule acrylate polymer precursors, a photo-initiator that has a large two-photon absorption cross-section at 780 nm and a photoinhibitor. After removing the solvent from the mixture, the final nanocomposite ink, a clean and transparent solution with light yellow colour, is produced as shown in the Fig. 1a inset. The as-synthesized nanocomposite ink stored in the dark can be kept stable for months without noticeable aggregation or settlement of the silica NPs. A small-angle X-ray scattering (SAXS) test was conducted on the nanocomposite ink, the result of which indicates that the silica NPs are well dispersed in the polymer precursors (more details are discussed in the Supplementary Information). The nanocomposite ink was then dropped onto a sapphire substrate that had been plasma cleaned and pretreated with proper sanitizer, producing a surface with moderate adhesion to the printed materials. Figure 1a illustrates a 2PP printer shaping the nanocomposite ink into designed 3D structures. In this process, a 780 nm, 100 fs laser beam is focused using a high-numerical-aperture, oil-immersive objective lens. The photo-initiator simultaneously absorbed two photons from the laser pulse and generated free radicals to initiate the polymerization process of the nanocomposite ink. In this step, the nanocomposite ink containing polymer precursors and

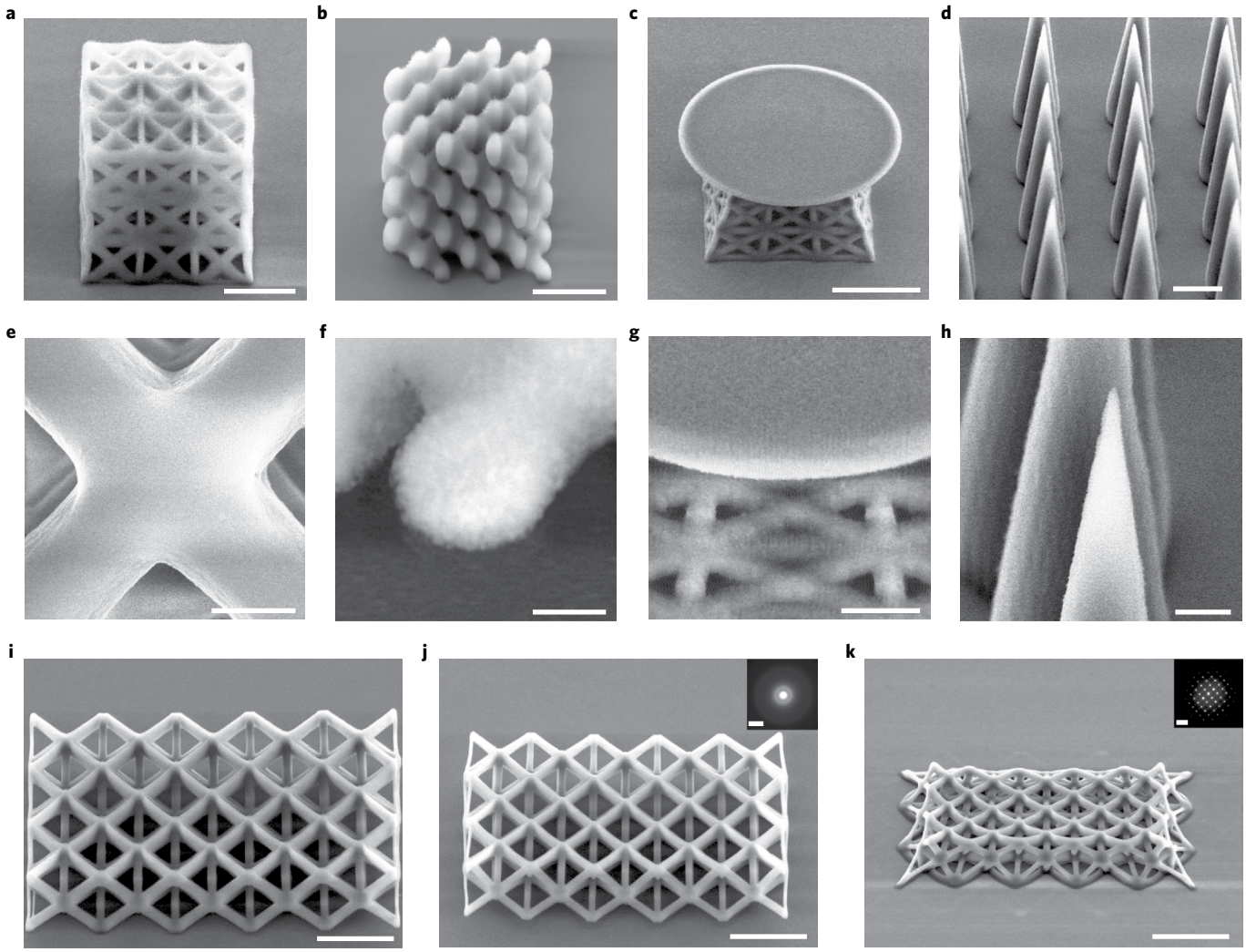

Fig. 2 | Microstructures of silica printed using the proposed 2PP-enabled AM technique. a–d, SEM images of 3D-printed fcc lattice truss structure (**a**; scale bar, 5 μm), diamond lattice truss structure (**b**; scale bar, 10 μm), disc-on-truss structure (**c**; scale bar, 10 μm) and needle array (**d**; scale bar, 10 μm). **e**, Zoomed-in top view of fcc lattice truss structure (scale bar, 400 nm). **f**, Zoomed-in top view of diamond lattice truss structure (scale bar, 1 μm). **g**, Zoomed-in top front view of disc-on-truss structure (scale bar, 2.5 μm). **h**, Zoomed-in top front view of needle array; tip radius, 230 nm (scale bar, 2.5 μm). **i**, SEM image of the as-printed octet truss structure before sintering (scale bar, 20 μm). **j**, SEM image of the printed octet truss structure sintered at 1,100 °C (scale bar, 20 μm); inset: TEM diffraction pattern showing amorphous structure (scale bar, 1 nm^{-1}). **k**, SEM image of the printed octet truss structure sintered at 1,300 °C (scale bar, 20 μm); inset: TEM diffraction pattern showing cristobalite structure (scale bar, 1 nm^{-1}).

silica NPs will be converted into a polymerized network with silica NPs. Due to the existence of the threshold effect[35] in 2PP, subwavelength critical resolution is achieved. By scanning the galvanometer transversely and moving the *z* axis with the piezoelectric stage, layers of sliced structures are additively formed and the final desired structures are printed (as shown in the bottom left insert of Fig. 1a). Immediately afterward, the as-printed materials are developed in propylene glycol monomethyl ether acetate solvent and rinsed with isopropyl alcohol. During this step, ultraviolet (UV), light-emitting diode lamps may be used to further cure the as-printed structures, and a critical point dryer can be optionally used to prevent collapse of the fine structures due to capillary forces.

The as-printed polymer/silica NP composite is then subjected to pyrolysis followed by sintering in a tube furnace. The organic substance in the product is decomposed and removed after heat treatment, leaving only aggregated silica NPs. As the temperature increases, silica NPs are converted into dense silica with different phases. In our experiments, it was revealed that sintering at 1,100 °C and 1,300 °C can produce high-quality amorphous glass and polycrystalline cristobalite (the bottom right inset of Fig. 1a), respectively (also refer to Supplementary Fig. 3 for detailed characterizations).

Figure 1b(iii),(iv) displays the optical and scanning electron microscopy (SEM) images of the final 3D-printed silica Rice Owl logo sintered at 1,100 °C with a 5 μm × 10 μm size. To explore the finest critical resolution, we printed isolated smooth lines (Fig. 1b(ii)). It was determined that the finest structure has a resolution of about 170 nm in width, showing that the proposed technique can achieve a resolution of sub-200 nm. Figure 2 displays typical SEM images of various printed 3D structures. These SEM images show that intricate structures with sub-200 nm resolution can be created using the above approach. Specifically, a 3 × 3 × 3 face cubic centre (fcc) lattice truss structure (Fig. 2a) composed of beams with width of 400 nm and a diamond lattice truss structure (Fig. 2b) with ellipsoid features of around 1 μm diameter were highlighted, presenting the remarkable printing capability of the strategy. More intricate structures such as a suspended disc-on-truss optical

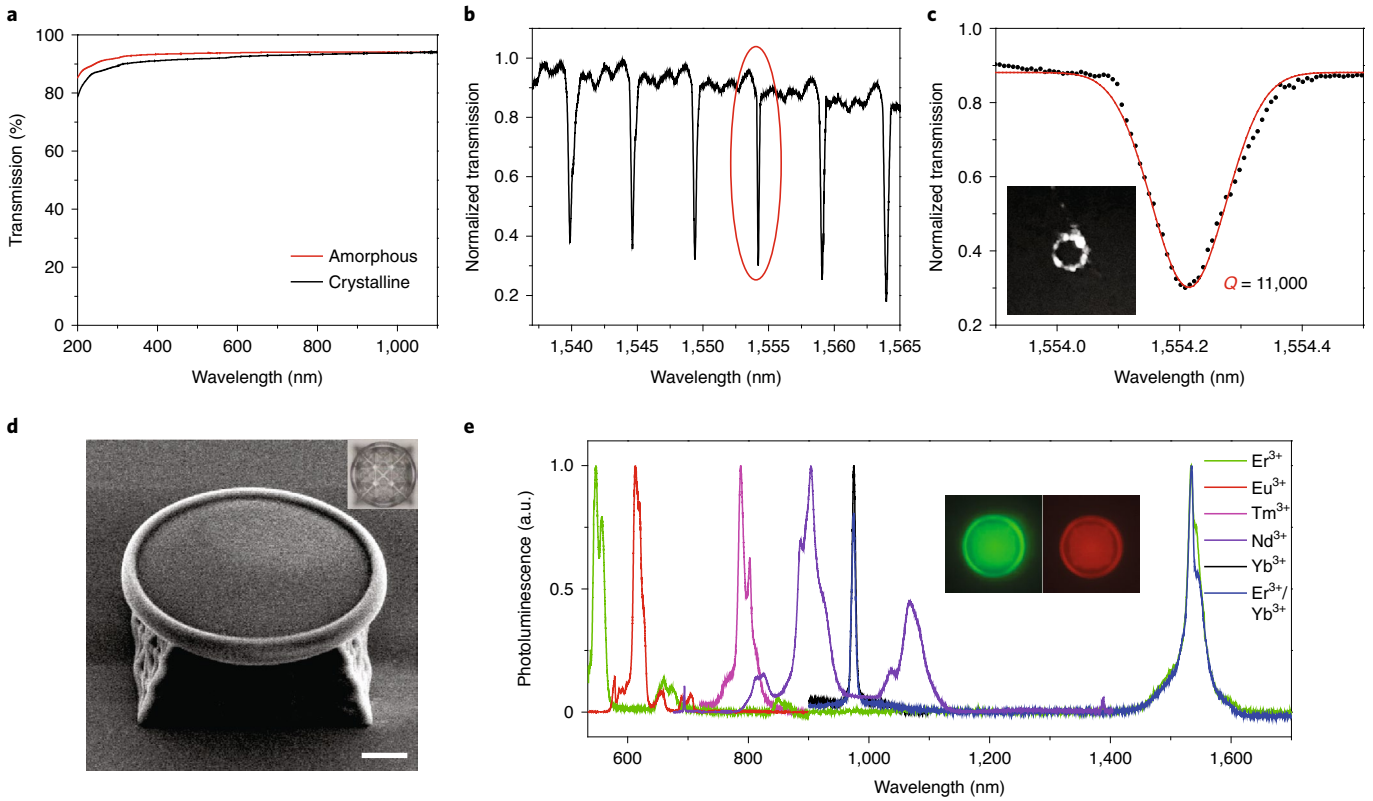

Fig. 3 | Optical applications of printed silica resonator. a, Transmission spectra of 3D-printed amorphous and crystalline silica. **b**, Transmission spectra of the 3D-printed micro-toroid optical resonator. **c**, Fitting of quality factor at 1,554.2 nm (peak highlighted with red oval in **b**). Inset: optical mode captured by infrared camera. **d**, SEM image of the printed micro-toroid optical resonator (scale bar, 10 µm); inset: optical image from the top. **e**, Photoluminescence of Er^{3+}-, Eu^{3+}-, Tm^{3+}-, Nd^{3+}- and Yb^{3+}-doped and Er^{3+}/Yb^{3+} (1:1)-codoped silica crystal in the visible to near-infrared range; inset: the Er^{3+}-doped micro-toroid optical resonator under 495 nm (left) and 592 nm (right) excitation and observed at 519 nm (left) and 614 nm (right) using a fluorescence microscope.

resonator with a disc diameter of 25 µm (Fig. 2c) and micro-needle arrays with sharp tips (Fig. 2d) can also be successfully fabricated.

SEM observations of a 3D-printed octet truss structure before and after sintering at two different temperatures were compared (Fig. 2i–k) to inspect the shrinkage and deformation induced by sintering, as the shrinkage rate is critical to maintain the as-designed structure and important for further optimization. Direct comparison between an as-sintered octet truss lattices at 1,100 °C (Fig. 2j) with their as-printed counterpart (Fig. 2i) revealed homogeneous linear shrinkage of about 15%. The shrinkage rate was relatively smaller than in previous work[20] using stereolithography. The improvement can be attributed to the higher loading concentration and good dispersity of NPs, which would greatly support the backbone of the as-printed structure. However, sintering at 1,300 °C will induce a large deformation resulting in the collapse of the as-designed structure, likely due to the melting process before crystallization and the thermal expansion mismatch between the sample and the substrate. The crystalline phase and elemental composition of the sintered silica were confirmed by transmission electron microscopy (TEM), X-ray diffraction and Raman spectra (Supplementary Fig. 3). The bright-field scanning TEM images in Supplementary Fig. 3a,d show that the printed silica structures are dense with no observable pores or cracks, while the energy-dispersive spectroscopy mapping in Supplementary Fig 3b,c,e,f demonstrates the homogeneous distributions of the Si and O elements. The diffraction patterns of the two samples (inset of Fig. 2j,k), pertaining to the amorphous and well-crystallized phases, agree well with the X-ray diffraction and Raman spectroscopy displayed in Supplementary Fig. 3g,i. X-ray photoelectron spectroscopy, shown in Supplementary Fig. 3h, confirms that the printed final materials are pure silica with the correct stoichiometric ratio for both samples.

Silica is a transparent material that is broadly applied in optical applications such as optical fibres, lenses and microphotonic components. To explore the unique optical capabilities of 2PP-printed structures, we measured the UV–visible transmission spectra of the printed amorphous and crystalline thin films with a thickness of around 2 µm, as plotted in Fig. 3a. The spectra indicate that the 3D-printed silica materials are highly transparent within the measured range between 200 nm to 1,100 nm without any visible absorption peaks. The printed amorphous silica exhibits overall higher transmission. The optical images of more printed transparent structures can be seen in Supplementary Fig. 4.

It is well recognized that traditional methods of fabricating silica microphotonic components are incapable of creating arbitrary 3D structures. However, the high-resolution 2PP-enabled AM technique opens doors for the fabrication of both passive and active microphotonic components, making the 3D printing of integrated photonic components feasible. Whispering gallery resonators are one of the fundamental components of integrated photonics, but the fabrication is challenging due to their 3D nature. A proof-of-concept micro-toroid optical whispering gallery resonator working in the 1,550 nm optical communication band was fabricated using our method (Fig. 3d). Compared to widely adopted techniques, which used optical lithography and XeF_2 plasma etching to make a suspended disc followed by forming the toroid by CO_2 laser reflow[36], the 3D-printed silica optical micro-toroid resonator on a tapered fcc lattice truss scaffold base offers two advantages. First, the structure of the supporting base can be made more mechanically robust by

proper design. In the previous method, the etching of the supporting structure could not be controlled. Second, the morphology of the toroid can be controlled precisely. In the previous method, the CO_2 laser reflow is not controllable, especially for discs with large diameters. By precisely manipulating the toroid morphology, we have fabricated resonators with different morphologies and high quality factors. Measurements of the micro-disc structure with zero toroid width, shown in Fig. 2c, indicate a quality factor of 5×10^3 (more measurement details can be found in the Supplementary Information and Supplementary Fig. 5). Figure 3b shows the transmission property, a standard resonance response with 4.8 nm free spectrum range, of the 3D-printed micro-toroid resonator around 1,550 nm. As fitted with a Lorentzian line-shape, the quality factor reaches 1.1×10^4 at 1,554 nm, which is comparable to that of the reported suspended silica optical resonators fabricated by the 2PP technique. Considering the large coupling loss in our measurements, the actual Q could be several orders of magnitude higher[37].

Furthermore, active photonic devices were fabricated by doping the nanocomposite ink with rare-earth elements. Similar doping strategies have been applied before to make coloured glasses[20,38,39]. However, active photonic components were not realized by those studies as they were by the submicrometre-resolution printing techniques shown in this work. Figure 3e shows the visible to near-infrared photoluminescence of as-printed Er^{3+}-, Eu^{3+}-, Tm^{3+}-, Nd^{3+}- and Yb^{3+}-doped and Er^{3+}/Yb^{3+} (1:1)-codoped amorphous silica film with concentrations of 1×10^{19} ions cm^{-3}. Each photoluminescence peak matches the atomic transition lines of individual rare-earth elements, and the inset images captured with a fluorescence microscope indicate that the doping is homogeneous, suggesting that the proposed technique is ideal for printing active microphotonic devices such as micro-lasers. More importantly, the proposed technique can fabricate rare-earth-doped micro-optical components with arbitrary shapes. Although the 2PP of polymer structures has been reported for active microphotonic devices by doping with organic dyes[40], their emission spectra are too broad for actual applications, and the stability of the polymer under high laser irradiation is a non-trivial issue.

In conclusion, we have developed a 2PP 3D-printing technique using the high loading of PEG-functionalized colloidal silica NPs. High-quality 3D silica structures with arbitrary shapes in amorphous glass or polycrystalline cristobalite form were created at sub-200 nm resolution using the 3D-printing and post-sintering technique. This method demonstrated flexible capabilities in doping/codoping of rare-earth elements, as well as achieving high-Q micro-toroid resonators, revealing the potential to build passive and active integrated microphotonic chips with silica via 3D printing. Further work to demonstrate sub-10 nm resolution with stimulated emission depletion[41] methods will bring exciting developments to the field. It is also envisioned that an arbitrary 3D structure of crystalline silicon can be fabricated by magnesium reduction[42] of printed crystalline silica, making the dream of 3D printing silicon chips a reality.

Online content

Any methods, additional references, Nature Research reporting summaries, source data, extended data, supplementary information, acknowledgements, peer review information; details of author contributions and competing interests; and statements of data and code availability are available at https://doi.org/10.1038/s41563-021-01111-2.

Received: 23 May 2020; Accepted: 24 August 2021;
Published online: 14 October 2021

References

1. Van Zant, P. *Microchip Fabrication* (McGraw-Hill Education, 2004).
2. Fortunato, E., Barquinha, P. & Martins, R. Oxide semiconductor thin-film transistors: a review of recent advances. *Adv. Mater.* **24**, 2945–2986 (2012).
3. Hsu, T. R. *MEMS and Microsystems: Design, Manufacture, and Nanoscale Engineering* (John Wiley & Sons, 2008).
4. Rossi, C. et al. Nanoenergetic materials for MEMS: a review. *J. Microelectromech. Syst.* **16**, 919–931 (2007).
5. Collot, L., Lefevre-Seguin, V., Brune, M., Raimond, J. M. & Haroche, S. Very high-Q whispering-gallery mode resonances observed on fused silica microspheres. *EPL* **23**, 327–334 (1993).
6. Okamoto, K. Progress and technical challenge for planar waveguide devices: silica and silicon waveguides. *Laser Photonics Rev.* **6**, 14–23 (2012).
7. Deal, B. E. & Grove, A. S. General relationship for the thermal oxidation of silicon. *J. Appl. Phys.* **36**, 3770–3778 (1965).
8. Inoue, K., Michimori, M., Okuyama, M. & Hamakawa, Y. Low temperature growth of SiO_2 thin film by double-excitation photo-CVD. *Jpn. J. Appl. Phys.* **26**, 805–811 (1987).
9. Quirk, M. & Serda, J. *Semiconductor Manufacturing Technology* (Prentice Hall, 2001).
10. Gokan, H., Esho, S. & Ohnishi, Y. Dry etch resistance of organic materials. *J. Electrochem. Soc.* **130**, 143–146 (1983).
11. Van der Heide, P. A. M., Baan Hofman, M. J. & Ronde, H. J. Etching of thin SiO_2 layers using wet HF gas. *J. Vac. Sci. Technol. A* **7**, 1719–1723 (1989).
12. Monk, D. J., Soane, D. S. & Howe, R. T. A review of the chemical reaction mechanism and kinetics for hydrofluoric acid etching of silicon dioxide for surface micromachining applications. *Thin Solid Films* **232**, 1–12 (1993).
13. Wong, K. V. & Hernandez, A. A review of additive manufacturing. *ISRN Mech. Eng.* **2012**, 208760 (2012).
14. Mueller, B. Additive manufacturing technologies—rapid prototyping to direct digital manufacturing. *Assem. Autom.* https://doi.org/10.1108/aa.2012.03332baa.010 (2012).
15. Camposeo, A., Persano, L., Farsari, M. & Pisignano, D. Additive manufacturing: applications and directions in photonics and optoelectronics. *Adv. Opt. Mater.* **7**, 1800419 (2019).
16. Chia, H. N. & Wu, B. M. Recent advances in 3D printing of biomaterials. *J. Med. Biol. Eng.* **9**, 4 (2015).
17. Skylar-Scott, M. A., Gunasekaran, S. & Lewis, J. A. Laser-assisted direct ink writing of planar and 3D metal architectures. *Proc. Natl Acad. Sci. USA* **113**, 6137–6142 (2016).
18. Hinton, T. J., Hudson, A., Pusch, K., Lee, A. & Feinberg, A. W. 3D printing PDMS elastomer in a hydrophilic support bath via freeform reversible embedding. *ACS Biomater. Sci. Eng.* **2**, 1781–1786 (2016).
19. Tan, Y. et al. 3D printing facilitated scaffold-free tissue unit fabrication. *Biofabrication* **6**, 024111 (2014).
20. Kotz, F. et al. Three-dimensional printing of transparent fused silica glass. *Nature* **544**, 337–339 (2017).
21. Lan, P. X., Lee, J. W., Seol, Y. J. & Cho, D. W. Development of 3D PPF/DEF scaffolds using micro-stereolithography and surface modification. *J. Mater. Sci. Mater. Med.* **20**, 271–279 (2009).
22. Lopes, A. J., MacDonald, E. & Wicker, R. B. Integrating stereolithography and direct print technologies for 3D structural electronics fabrication. *Rapid Prototyp. J.* **18**, 129–143 (2012).
23. Xing, J. F., Zheng, M. L. & Duan, X. M. Two-photon polymerization microfabrication of hydrogels: an advanced 3D printing technology for tissue engineering and drug delivery. *Chem. Soc. Rev.* **44**, 5031–5039 (2015).
24. Tan, D. et al. Reduction in feature size of two-photon polymerization using SCR500. *Appl. Phys. Lett.* **90**, 071106 (2007).
25. Juodkazis, S., Mizeikis, V., Seet, K. K., Miwa, M. & Misawa, H. Two-photon lithography of nanorods in SU-8 photoresist. *Nanotechnology* **16**, 846–849 (2005).
26. Ovsianikov, A. et al. Ultra-low shrinkage hybrid photosensitive material for two-photon polymerization microfabrication. *ACS Nano* **2**, 2257–2262 (2008).
27. Brigo, L. et al. 3D nanofabrication of SiOC ceramic structures. *Adv. Sci.* **5**, 1800937 (2018).
28. Schmidt, J. et al. Multiscale ceramic components from preceramic polymers by hybridization of vat polymerization-based technologies. *Addit. Manuf.* **30**, 100913 (2019).
29. Chandrappan, J. et al. Doping silica beyond limits with laser plasma for active photonic materials. *Opt. Mater. Express* **5**, 2849–2861 (2015).
30. El-Ganainy, R., Khajavikhan, M., Christodoulides, D. N. & Ozdemir, S. K. The dawn of non-Hermitian optics. *Commun. Phys.* **2**, 37 (2019).
31. Zhong, T. et al. Nanophotonic rare-earth quantum memory with optically controlled retrieval. *Science* **357**, 1392–1395 (2017).
32. Mohanty, S. R. A relationship between heat conductivity and viscosity of liquids. *Nature* **168**, 42 (1951).
33. Lin, B. & Zhou, S. Poly (ethylene glycol)-grafted silica nanoparticles for highly hydrophilic acrylic-based polyurethane coatings. *Prog. Org. Coat.* **106**, 145–154 (2017).

34. Kotz, F. et al. Two-photon polymerization of nanocomposites for the fabrication of transparent fused silica glass microstructures. *Adv. Mater.* **33**, 2006341 (2021).
35. Farsari, M. & Chichkov, B. N. Two-photon fabrication. *Nat. Photon.* **3**, 450–452 (2009).
36. Hossein-Zadeh, M. & Vahala, K. J. Free ultra-high-Q microtoroid: a tool for designing photonic devices. *Opt. Express* **15**, 166–175 (2007).
37. Liu, Z. P. et al. Direct laser writing of whispering gallery microcavities by two-photon polymerization. *Appl. Phys. Lett.* **97**, 211105 (2010).
38. Moore, D. G., Barbera, L., Masania, K. & Studart, A. R. Three-dimensional printing of multicomponent glasses using phase-separating resins. *Nat. Mater.* **19**, 212–217 (2020).
39. Nguyen, D. T. et al. 3D-printed transparent glass. *Adv. Mater.* **29**, 1701181 (2017).
40. Grossmann, T. et al. Direct laser writing for active and passive high-Q polymer microdisks on silicon. *Opt. Express* **19**, 11451–11456 (2011).
41. Gan, Z., Cao, Y., Evans, R. A. & Gu, M. Three-dimensional deep sub-diffraction optical beam lithography with 9 nm feature size. *Nat. Commun.* **4**, 2061 (2013).
42. Richman, E. K., Kang, C. B., Brezesinski, T. & Tolbert, S. H. Ordered mesoporous silicon through magnesium reduction of polymer templated silica thin films. *Nano Lett.* **8**, 3075–3079 (2008).

Methods

Propylene glycol monomethyl ether acetate (PGMEA), acetone, isopropanol alcohol, ethylene glycol (99.8%), trimethylolpropane ethoxylate triacrylate, poly (ethylene glycol) diacrylate, 4,4′-bis (diethylamino) benzophenone (≥99%), hydroquinone (≥99%), erbium (III) chloride hexahydrate (99.9%), ytterbium (III) chloride hexahydrate (99.9%), thulium (III) chloride hexahydrate (99.9%) and europium (III) chloride hexahydrate (99.9%) were purchased from Sigma-Aldrich. PEG-functionalized silica nanoparticles in a colloidal solution with methyl ethyl ketone as the solvent (MEK-AC-2140Z) were provided by Nissan Chemical America Corporation. Neodymium (III) chloride hydrate (99.9%) was purchased from Alfa Aesar. A two-sided polished sapphire wafer was purchased from University Wafer.

Preparation of nanocomposite ink. Trimethylolpropane ethoxylate triacrylate (333 mg) was mixed with poly (ethylene glycol) diacrylate (666 mg) by magnetic stirring at room temperature for 5 min. Then 1,600 mg of colloidal silica solution was slowly added into the mixture under magnetic stirring. After the mixture became clear and transparent, 5 mg of hydroquinone was added to the mixture to inhibit the reaction of polymer precursors. The mixture was then kept in a vacuum drying oven at 60 °C for 2 hours to totally evaporate the solvent. At last, 10 mg of 4,4′-bis (diethylamino) benzophenone was added to the mixture. The prepared precursor was sonicated for 30 min until the resulting solution became transparent.

To prepare the precursor doped with a rare-earth element, 50 mg of rare-earth salts were selectively added to the precursor before the photo-initiator was added. Sonication was applied to accelerate the dissolving process; 500 mg of ethylene glycol could be selectively used to help dissolve the erbium chloride.

2PP 3D-printing process. Silica/photopolymer composite microstructures were fabricated by a commercial 2PP AM system (Nanoscribe Photonic Professional GT). Oil-immersion-mode objective lenses (63×, numerical aperture, 1.4 or 25×, numerical aperture, 0.8) were chosen to do the printing. First, a sapphire wafer was sonicated in acetone for 15 min and rinsed by isopropanol alcohol three times. The wafer was then cleaned by O_2 plasma for 15 min to totally remove contamination. Nanocomposite ink was then dropped onto the sapphire substrate and loaded into the Nanoscribe AM machine. During the printing process, laser power and laser scanning speed were set to be 15–20 mW and 4–5 mm s^{-1}, respectively. After the printing process, the wafer was immersed in PGMEA for 5 min to dissolve the unpolymerized precursor and then immersed in isopropanol alcohol for 5 min to remove residual PGMEA. Then a 100 W UV light-emitting diode lamp was used to further solidify the printed structure for another 5 min (optional). Finally, the sample immersed in isopropanol alcohol was dried out by critical point dryer to avoid the collapsing of the printed microstructure due to the surface tension of the solvent.

Pyrolysis and sintering process. Heat treatment was used to remove the polymer, sinter the silica NPs and change the crystallinity of the produced structures. The heat treatment process was carried out in a tube furnace with nitrogen as the protection gas under low pressure. Before the heat treatment, several gas purge cycles were carried out to remove the contaminants and reactive gases in the tube. Next the temperature was set to increase from room temperature to the desired temperature at a speed of 1 °C min^{-1}. When the temperature reached 300 °C, 600 °C, 1,000 °C and 1,100 °C, it was held for 180 min, 120 min, 500 min and 180 min, respectively, in the case of the amorphous final structures. In the crystalline case, the final temperature was further increased to 1,300 °C with a hold time of 240 min. Finally, the furnace was slowly cooled down to room temperature with the speed of 2 °C min^{-1} to prevent cracking during the cooling process. The detailed temperature versus time curve is shown in Supplementary Fig. 6.

Sample characterizations. TEM observation of the colloidal silica was carried out using an FEI Titan Themis3; scanning TEM characterization of printed materials was done with a JEOL 2100. The instrument for X-ray diffraction was a Rigaku D/Max Ultima II. A PHI Quantera X-ray photoelectron spectroscopy instrument was used to measure the X-ray photoelectron spectra. The UV–visible transmission spectrum in Fig. 3a was measured using a Cary 50 UV–visible spectrophotometer. Raman spectroscopy of the printed materials and photoluminescence of Er^{3+}-, Eu^{3+}-, Tm^{3+}-, Nd^{3+}- and Yb^{3+}-doped and Er^{3+}/Yb^{3+} (1:1)-codoped SiO_2 crystal was measured using a Renishaw confocal Raman spectrometer under 532 nm or 785 nm excitation. The optical microscope images in Figs. 1b and 3d and the fluorescence image in Fig. 3e were measured with a Zeiss LSM 710 confocal microscope.

Data availability

The data that support the findings of this study are available from the corresponding authors upon reasonable request. Source data are provided with this paper.

Acknowledgements

X.W., B.Z., W.W., H.G., Q.F., C.N. and J.L. gratefully acknowledge the financial support by the Welch Foundation grant C-1716. J.B. gratefully acknowledges the financial support by the Welch Foundation grant E-1728. This work was conducted in part using resources of the Shared Equipment Authority at Rice University. We thank J. Li at the Shared Equipment Authority of Rice University for help with the SAXS experiments. We also thank X-M. Lin at Argonne National Laboratory for help with Fourier transform infrared spectroscopy experiments.

Author contributions

X.W., J.L. and P.M.A. designed the experiment; X.W. and B.Z. performed the nanocomposite ink preparation and 2PP printing; X.W., B.Z., W.W., H.G., G.G., Y.Z., Q.F., C.N. and X.Z. contributed to sample characterization; F.Y. and J.T.R. helped with the optical resonator test; and S.Y. and J.B. helped with the photoluminescence measurements.

Competing interests

The authors declare no competing interests.

Additional information

Supplementary information The online version contains supplementary material available at https://doi.org/10.1038/s41563-021-01111-2.

Correspondence and requests for materials should be addressed to Weipeng Wang, Jacob T. Robinson, Pulickel M. Ajayan or Jun Lou.

Peer review information *Nature Materials* thanks Paolo Colombo, Kunal Masania and Bastian Rapp for their contribution to the peer review of this work.

Reprints and permissions information is available at www.nature.com/reprints.